# In situ synthetic functionalization of a transmembrane protein manopore

# *In situ* Synthetic Functionalization of a Transmembrane Protein Nanopore

*Stefan Borsley and Scott L. Cockroft**

EaStCHEM School of Chemistry, University of Edinburgh, Joseph Black Building, David Brewster Road, Edinburgh, EH9 3FJ, U.K.

ABSTRACT: Monitoring current flow through a single nanopore has proved to be a powerful technique for the *in situ* detection of molecular structure, binding and reactivity. Transmembrane proteins, such as α–hemolysin, provide particularly attractive platforms for nanopore sensing applications due to their atomically precise structures. However, many nanopore applications require the introduction of functional groups to tune selectivity. To date, such modifications have required genetic modification of the protein prior to functionalization. Here we demonstrate the *in situ* synthetic modification of a wild-type α-hemolysin nanopore embedded in a membrane. We show that reversible dynamic covalent iminoboronate formation and the resulting changes in the ion current flowing through individual nanopores can be used to map the reactive behavior of lysine residues within the nanopore channel. Crucially, the modification of lysine residues located outside the nanopore channel were found not to affect the stability or utility of the nanopore. Finally, knowledge of the reactivity patterns enabled the irreversible functionalization of a single, assignable lysine residue within the nanopore channel. The approach constitutes a

simple, generic tool for the rapid, *in situ* synthetic modification of protein nanopores that circumvents the need for prior genetic modification.

KEYWORDS: nanotechnology; single-molecule; nanopore; protein modification; dynamic covalent chemistry;

Nanopore-based approaches have proved to be a powerful technique for examining processes at the single-molecule level.[1,2] Monitoring the current flow through a single nanopore enables the *in situ* characterization of molecular structure,[3] binding[4] and even reactivity.[5-8] Nanopores can be broadly classed as either solid-state or biological nanopores.[9,10] Solid-state nanopores are often formed by top-down approaches as exemplified by track-etched polymer membranes,[11-15] or those formed by focused electron[16,17] or ion[16,18] beams. Meanwhile, arrays of solid-state pores may be formed in self-assembled colloidal membranes[19] or templated mesoporous membranes.[20-24] Solid state nanopores are generally robust[9] and stable to chemical modifications[25-27] that may be used to introduce chiral,[28] pH-responsive[29] and photo-switchable functionalities.[30] In contrast, biological nanopores are formed by the bottom-up self-assembly of proteins, to yield atomically precise and reproducible channels, albeit, with more limited options for chemical modification compared to their solid-state counterparts. While the precision and reproducibility of solid-state nanopore manufacture continues to improve, and new strategies for the bottom-up synthesis of nanopores,[31] such as DNA origami[32-34] hold much promise, proteins currently provide the most reproducible and reasonably robust nanopores.

α-Hemolysin (α-HL) is the best-studied biological nanopore.[35] α-HL is expressed by *Staphylococcus aureus* and spontaneously assembles to form heptameric, membrane-spanning channels. Numerous sensing applications of α-HL require modification of the protein to instil specific functionality. Cyclodextrin adapters may be covalently or non-covalently bound,[36-39] but genetic modification of the nanopore is required to ensure robust, long-lived functionalization. Further functionality has been introduced to α-HL through genetic modification to introduce a single cysteine residue.[40] This cysteine residue may then be targeted by a well-developed toolkit for post-translational chemical modification, including disulfide

chemistry and Michael additions.[41] The reactivity of cysteine-containing mutant α-HL has been exploited for molecular detection[6] and for probing reactivity.[42] More recently, native chemical ligation has been used to append synthetic functionalities,[43] which may be further modified by additional reactions. While the applications of such modified nanopores have been remarkable, genetic modification requires specific expertise, may be time-consuming, or give rise to protein-folding and purification issues.[44] Such limitations make rapid prototyping of modified pores difficult. To date, synthetic post-translational modification of protein transmembrane channels has most commonly been achieved on genetically modified pores,[8,43] or exceptionally by *N*-terminus functionalization.[45] While the specificity of synthetic chemical modification of a protein nanopore is unlikely to match that offered by genetic mutation or native chemical ligation, rapid access to sophisticated hybrid nanopores *via in situ* chemical modification is an extremely attractive prospect. Indeed, a number of well-established methods for synthetically modifying proteins have been developed, with reactions at nucleophilic lysine residues being particularly well-exploited.[41,46-48] Although the modification of a protein while captured within a nanopore has recently been demonstrated,[49] the *in situ* modification of the pore itself remains unexplored.

Here, we investigate the feasibility of selectively functionalizing lysine residues within the channel of a single wild-type α-HL nanopore whilst embedded within a lipid membrane (Figure 1). Dynamic covalent chemistry and ion current recordings were used to probe the reactivity of lysine residues within the pore channel (Figures 2 to 6), and the robustness of the nanopore to synthetic modification. Finally, reactions targeting the irreversible modification of single, assignable lysine residues within an individual nanopore were performed (Figure 7).

## Results and Discussion

### Approach for characterizing functionalization of lysine residues within the nanopore

Examination of the crystal structure[50] of the widely employed α-HL nanopore reveals three rings of lysine residues within the pore channel; one at the *cis*-side (d = 2.5 nm), one at the *trans*-side (d = 2.1 nm), and one at the constriction site, midway through the channel (d = 1.5 nm) (Figures 1A–B, S41). We envisaged that it would be possible to visualize reactions at these lysine residues *via* blockages in the ionic current flowing through a single nanopore under an applied potential. Reactions on the lysine residues at the narrow constriction site of the nanopore were expected to give the largest current blockages. Meanwhile, reactions occurring at exterior lysine residues should be of little consequence in typical nanopore sensing applications that detect events occurring within the pore, provided that the integrity of the channel is maintained (*vide infra*).

Ultimately, the irreversible modification of an individual lysine residue, for example *via* amide formation (Figure 1C), at an assignable location within the nanopore would be highly desirable, enabling access to sophisticated, specialized nanopores. However, before seeking to attain this objective, it is first pertinent to understand the reactivity of the lysine residues within the nanopore in question. The single-molecule nature of nanopore observations means that large data sets must be generated to render data statistically significant, and to allow confidence in interpreting ion current changes associated with such functionalization reactions. As noted by Bayley *et al*.,[8,43] the reversible nature of dynamic covalent chemistry enables vast numbers of individual reactions to be sampled in a single nanopore experiment. Lewis acid-stabilized Schiff

base formation[51-54] of an iminoboronate with the lysine residues (Figure 1D) was selected as an attractive reversible reaction for thoroughly characterizing the *in situ* functionalization of α-HL.

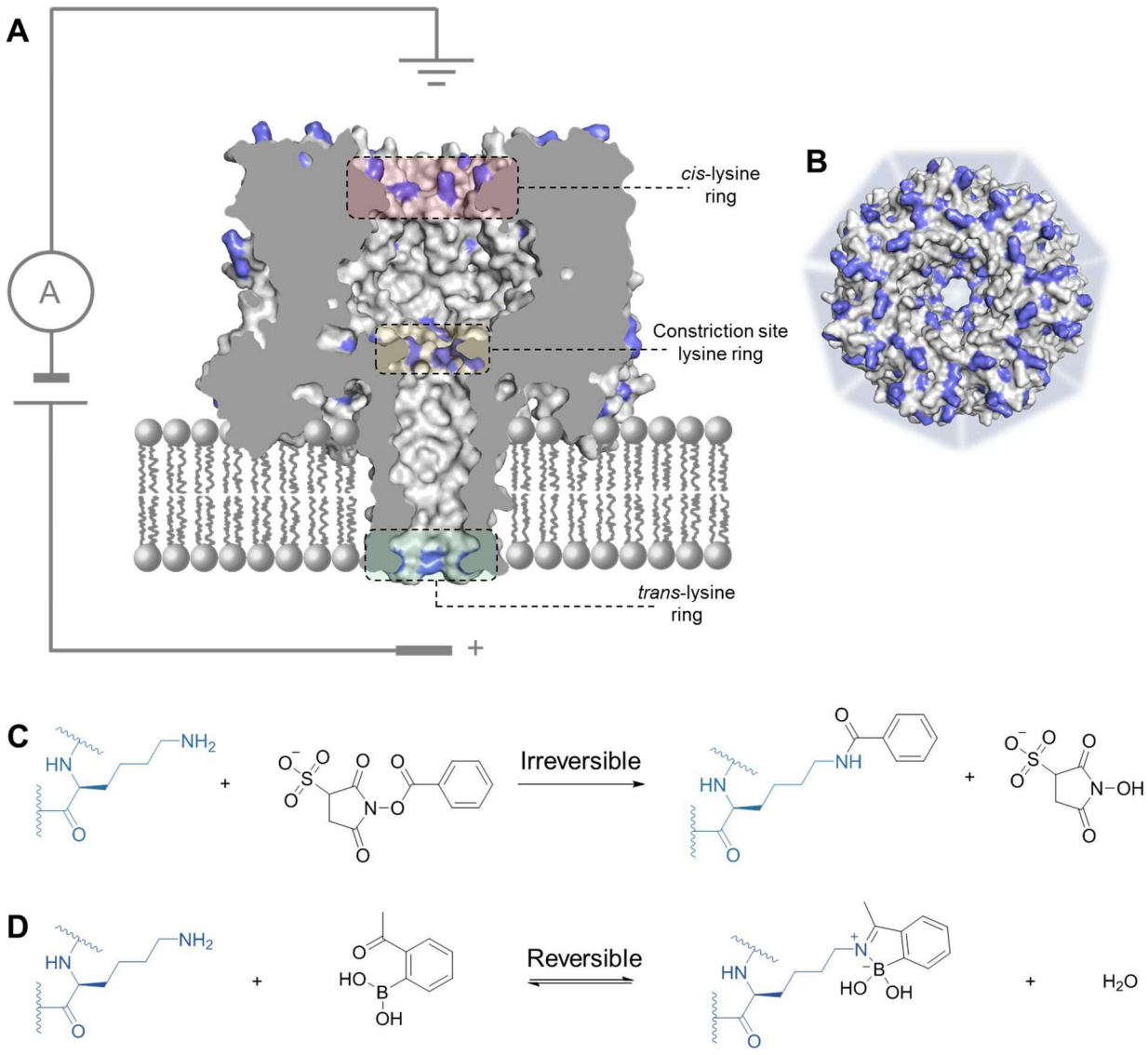


**Figure 1** (**A**) Cross section of the α-hemolysin crystal structure with all lysine residues highlighted in blue, showing the positioning of the electrodes in the experimental set-up. (**B**) Top view of α-hemolysin crystal structure highlighting the seven-fold symmetry of the heptameric assembly. (**C**) Scheme of irreversible amide formation with lysine residues. (**D**) Scheme of reversible iminoboronate formation with lysine residues.

**Reversible iminoboronate modification of an individual protein nanopore**

In a typical experiment, a single α-HL nanopore was inserted into a membrane under an applied potential in 1 M KCl, 30 mM phosphate at pH 8.0 (Figure S2, S7). Reversible step-wise blockages in the free pore current were observed upon addition of 2-acetylphenylboronic acid (final concentration ~3.2 μM, Figure 1D) to the *cis*-side of the membrane under an applied positive potential (Figures 2, S8). These reversible step-wise changes in the ion current were found to depend on both the concentration of the boronic acid (Figures S17–S25), and the known pH-responsiveness of the reaction[52] (Figures S8–S10, S12–S16 and accompanying text), allowing unambiguous attribution to iminoboronate formation. Additional control experiments with compounds lacking either the boronic acid (Figure S33) or carbonyl functionalities (Figure S34) did not produce any effect on the current trace, further indicating that the observed reversible blockages were indeed due to dynamic covalent iminoboronate formation. Following addition of 2-acetylphenylboronic acid (Figure S11), both the membrane (Figure S35) and the pore remained stable for hours, with no change in free pore noise (Figure S40), indicating that reaction on the exterior of the pore did not affect the protein stability, nor was there any allosteric effect on the nature of the channel.

Closer examination of the ion current traces upon addition of 2-acetylphenylboronic acid to the *cis*-side of the bilayer (Figures 2, S8, S11) revealed two classes of ion current blockage ($I_b/I_o$) change: large steps (≈13% of the free pore current, colored bars in Figure 2) and smaller steps (≈1% of the free pore current within each of the colored bars in Figure 2). It can be reasonably concluded that the observed large current-steps corresponded to iminoboronate formation at the lysine ring found at the constriction site of the nanopore, while the smaller changes correspond to modification of the much larger *cis*-lysine ring. Indeed, the decrease in current of ≈13% is in

excellent agreement with the predicted current flow for a blockage of this size from a simple geometric model[55] (Figure S44 and associated text). When 2-acetylphenylboronic acid was added to the *trans*-side of the pore under an applied negative potential, the ≈13% blockages corresponding to iminoboronate formation at the central lysine ring were still observed, but the ≈1% blockages of the free pore current were not (Figures S28, S29). Instead, a new series of blockages corresponding to ≈9% of the free pore current were observed, which can be attributed to reaction at the *trans*-lysine ring (bottom of Figure 1A and Figures S28, S29). Interestingly, reactions at the *trans*-lysine ring were not observed upon addition of 2-acetylphenylboronic acid to the *cis*-side (Figure 3A), and likewise, addition to the *trans*-side did not result in iminoboronate formation at the *cis*-lysine ring (Figure 3B). This is likely a result of the negligible concentration of 2-acetylphenylboronic acid on the opposite side of the membrane.

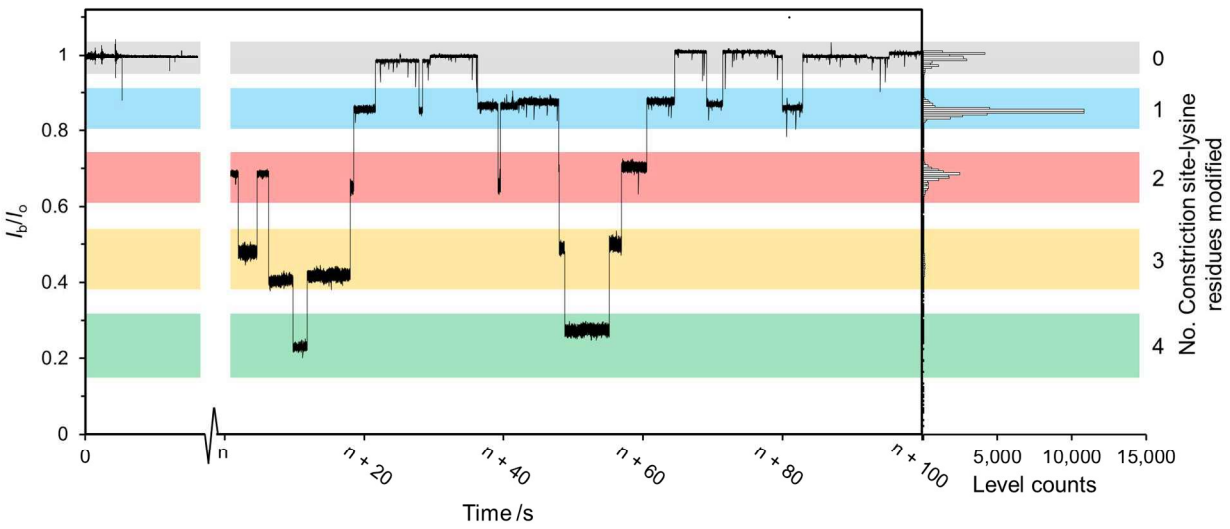


**Figure 2** A sample ion current trace (1 M KCl, 30 mM phosphate, pH 8.0, +100 mV, 298 K) generated following the addition of 2-acetylphenylboronic acid to the *cis*-side of the bilayer. Figure S11 the initial diffusion-controlled lag period. Discrete steps are observed, with up to four large steps (colored bars). Histogram of level counts for all data is shown to the right of the trace.

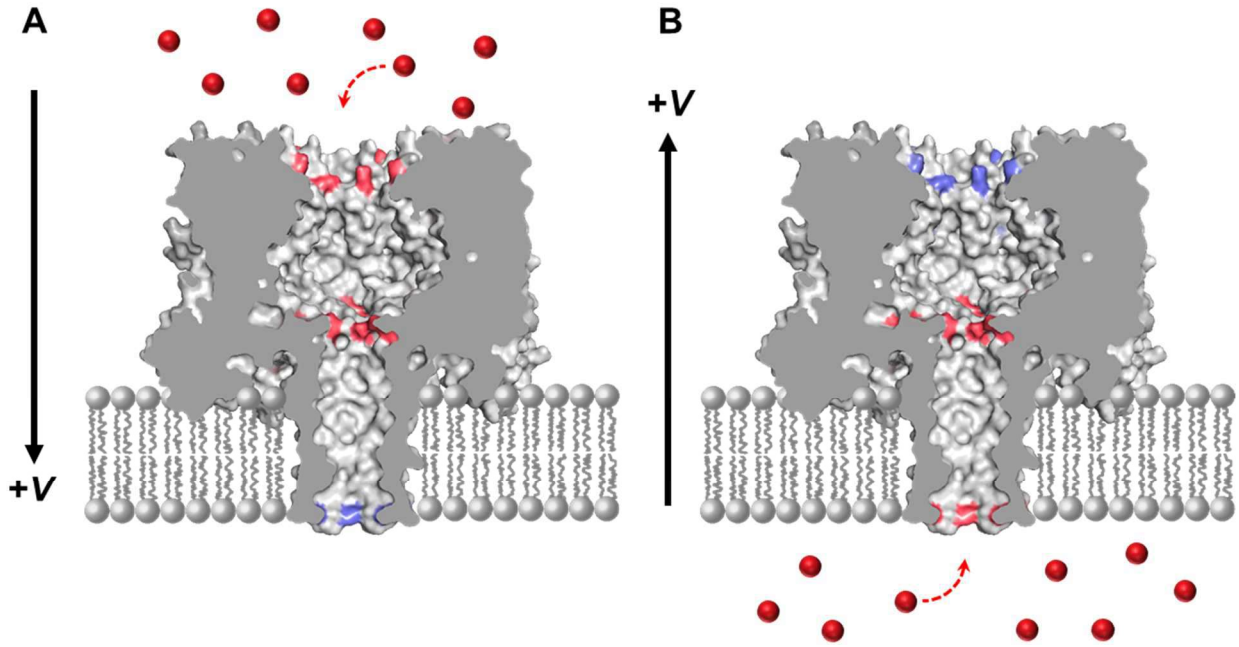


**Figure 3** Cross section of the α-hemolysin crystal structure, illustrating the reactive lysine ring locations, dependant on whether the 2-acetylboronic acid is added to the *cis*-(**A**) or the *trans*-side of the pore (**B**). Reactive lysine residues are colored red, unreactive lysine residues are colored blue.

Up to four large steps can be seen in the current traces resulting from the addition of 2-acetylphenylboronic acid to the *cis*-side of the bilayer (colored bars, Figure 2), which can be ascribed to sequential modification of four lysine residues at the constriction site (Figure 1B, middle). The full traces were analyzed using a single-channel search protocol (see Methods). Five discrete distributions, corresponding to iminoboronate formation at 0 (gray background), 1 (blue), 2 (red), 3 (yellow) and 4 (green) constriction-site lysine residues were revealed (Figure 2) with each state having an average half-life of approximately 3 s (Figure S10). Molecular modelling demonstrates the steric hindrance upon formation of successive iminoboronates at the constriction site (Figure S45). This steric hindrance is likely the reason why the formation of five or more iminoboronates was not observed, while the formation of three and four iminoboronates

is less frequently observed. Changing the reagent from 2-acetylphenylboronic acid to (2-formyl-4,5-dimethoxyphenyl)boronic acid revealed similar, reversible current blockages (Figure S18). However, the amplitude of the current blockages was larger (≈17%) (Figures S30–S32), consistent with the larger size of (2-formyl-4,5-dimethoxyphenyl)boronic acid compared to 2-acetylphenylboronic acid (Figure S44 and associated text). Furthermore, fewer and shorter blockages were observed compared to that seen for the smaller reagent, indicating a lower equilibrium constant. Indeed, this observation agreed with control experiments performed in free solution using NMR spectroscopy that revealed a lower equilibrium constant for the formation of the formyliminoboronate over the acetyliminoboronate in free solution (Figure S3–S6).

**The kinetics of iminoboronate modification at a single lysine residue**

The ability to observe discrete current levels for both the unreacted pore and a pore containing a single iminoboronate modification (Figures 4A and S26) allows the determination of kinetic parameters relating to a single reaction occurring at any one of the seven constriction site-lysine residues. Such an analysis was possible because reactions occurring at only a single constriction site-lysine residue were dominant at low concentrations of the reagent (e.g. 73% of events at 3.2 μM acetyliminoboronate, Figure S8). Notably, such a single-molecule approach reveals the distribution of state durations (Figure 4B,C), that would otherwise be inaccessible using ensemble techniques. Frequency-count histograms for the duration of the single-molecule states were fitted to single exponential decay functions as the concentration of the reagent was varied between 0 and 3.2 μM (e.g. Figure 4B,C and Figures S17–S24, S27 for other concentrations). Commensurate with the bimolecular nature of the reaction, the half-life of a single iminoboronate ($\tau_{off}$) was found to be independent of reagent concentration (Figure 4E), whereas the half-life of the unmodified pore ($\tau_{on}$) was linearly dependent on the concentration (Figure

4D). Thus, the rate constant of association at any one of the seven constriction site-lysine residues, $k_{on} = 1/\tau_{on}$[reagent], and dissociation, $k_{off} = 1/\tau_{off}$, were determined to be $7.7 \pm 0.8 \times 10^4$ $M^{-1}$ $s^{-1}$ and $0.21 \pm 0.01$ $s^{-1}$ respectively, corresponding to an association constant ($K_a = \underline{k}_{on}/k_{off}$) of $3.7 \pm 0.5 \times 10^5$ $M^{-1}$ under the conditions employed (Figure 4D, E). Due to the non-equilibrium conditions employed (in which a voltage of 100 mV is applied across the nanopore), the association constant observed in our single-molecule experiments is two orders of magnitude higher than that observed in bulk solution at equilibrium (Figure S5).

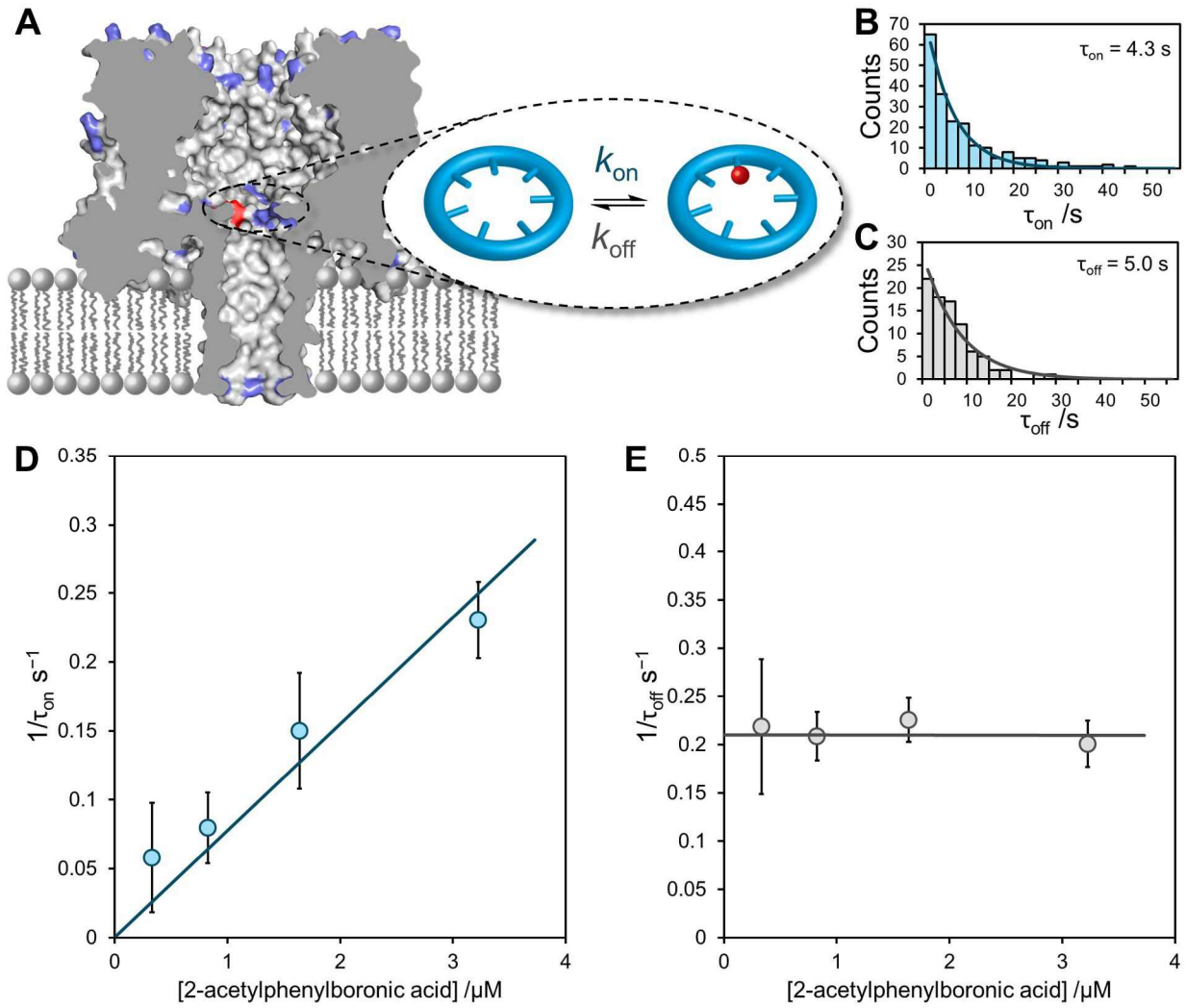


**Figure 4** (**A**) Kinetics of reversible iminoboronate formation/hydrolysis at a single constriction site-lysine residue. (**B**) Free-pore lifetime, $\tau_{on}$ and (**C**) single-iminoboronate lifetime, $\tau_{off}$ distributions in the presence of 3.2 μM 2-acetylphenylboronic acid, 1 M KCl, 30 mM phosphate, at pH 8.0, +100 mV, and 298 K. (**D**) Concentration dependence of $1/\tau_{on}$. The rate constant $k_{on}$ was obtained from the slope of the linear fit. (**E**) Concentration dependence of $1/\tau_{off}$. The rate constant $k_{off}$ was obtained from the intercept of the graph. Extended current traces for each concentration are provided in Figures S8, S17, S19, S21.

**Probing the relative positions of iminoboronate modification of a protein nanopore**

Having performed a complete kinetic analysis of the reactivity at a single constriction site-lysine residue, we next characterized situations in which multiple constriction-site residues were modified. As noted above, five major current levels can be assigned to 0, 1, 2, 3 or 4 iminoboronate modifications (colored bars in Figure 2). As expected, the scatter plot of the residual current $I_b/I_o$ *vs* level duration (Figure 5A) and the cumulative level duration histogram (Figure 5B) both showed a single distribution for iminoboronate modification at a single constriction site-lysine residue. In contrast, the data for 2 (red background) and 3 (yellow background) constriction-site modifications did not form a single distribution, raising the possibility that the relative positions of multiple modifications can be detected. Unfortunately, further analysis of the histograms in Figure 5B is complicated by ~1% current variations arising from iminoboronate formation at the *cis*-lysine ring (see previous section). However, it was possible to observe short series of events in which reactions only occurred at the constriction site-lysines, and no concurrent reactions occurred at the *cis*-lysines (*i.e.* no ~1% current variations were observed). For example, Figure 5C shows a series of events in which the current level transitions from a state containing 2 iminoboronate modifications (red background), to 1 (blue background), and back to 2 (red background), but at a current that is 3% different from the earlier state (dashed red lines). Similarly, Figure 5D shows a transition from 2 iminoboronate modifications (red background), to 3 (yellow background) and back to 2 (red background), this time at a current that is 8% different from the earlier state (dashed red lines). The current differences of these sub-levels within the major band (dashed red lines in Figures 5C and 5D) are substantially larger than the ~1% changes caused by iminoboronate formation at the *cis*-lysine ring, indicating that they relate to differences in the relative position of the modifications.

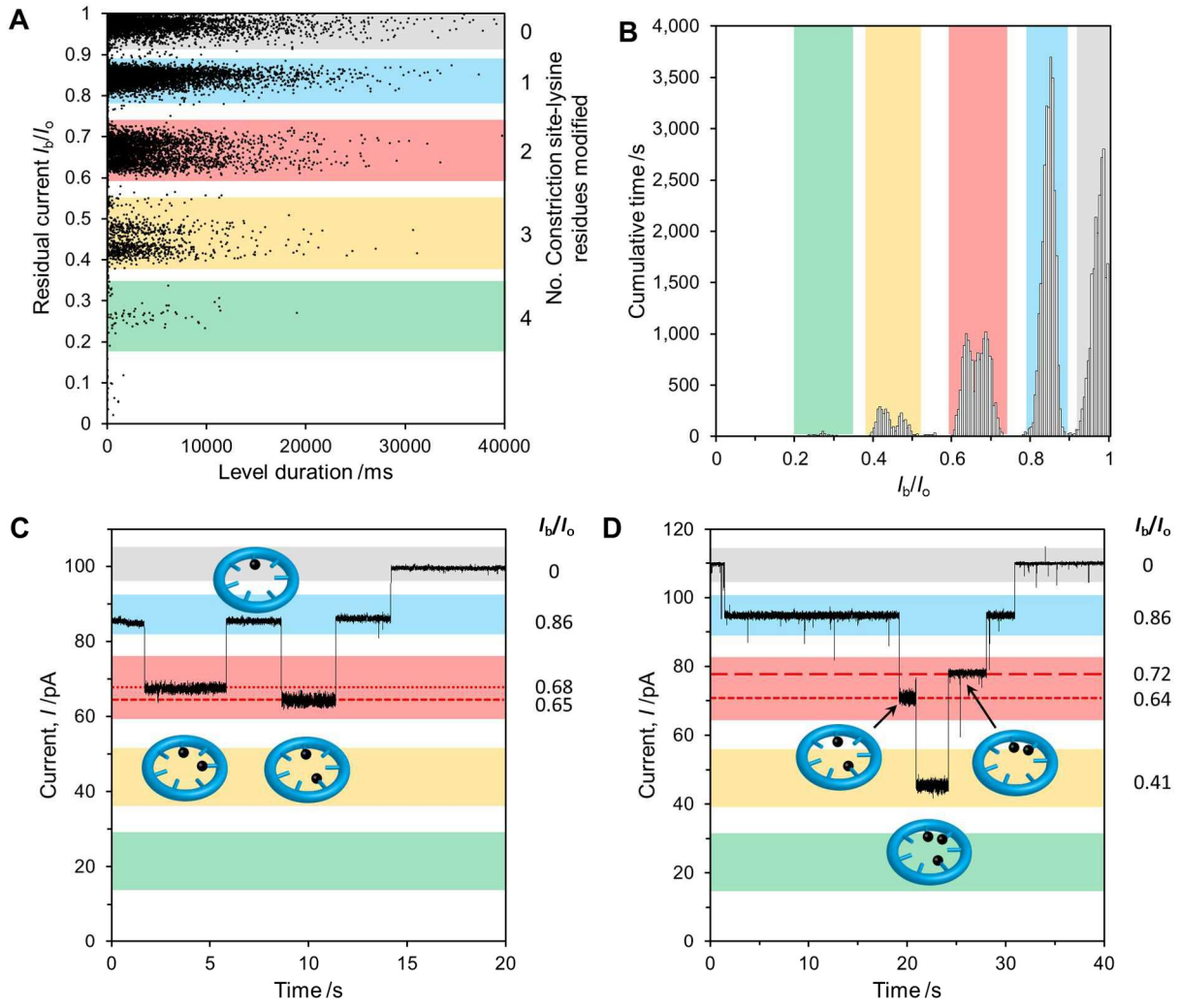


**Figure 5** (**A**) Scatter plot of current levels *vs* level durations and (**B**) cumulative time histogram generated on the addition of 2-acetylphenylboronic acid (3.2 μM) to the *cis*-side of the bilayer (1 M KCl, 30 mM phosphate, pH 8.0, +100 mV, 298 K). Sample traces where no small steps relating to *cis*-lysine iminoboronate formation are visible have been selected. The current trace steps from two constriction site lysine modifications to one and back to two (**C**), and two to three and back to two (**D**). In both cases the current level relating to two modified lysines changes. Cartoon insets illustrate potential positions that are responsible for the change in current level.

However, sequences of events such as those shown in Figures 5C and 5D occurred only ~10 times per hour (3.2 μM 2-acetylphenylboronic acid), making a more detailed interpretation of the current levels challenging. This difficulty can be circumvented by examining the *major changes* in ion currents ($|\Delta I_b/I_o|$), as opposed to the absolute current levels (Figure 6A). Such an approach greatly simplifies analysis of the reactivity patterns, revealing the states of the lysines at the constriction site (Figure 6).

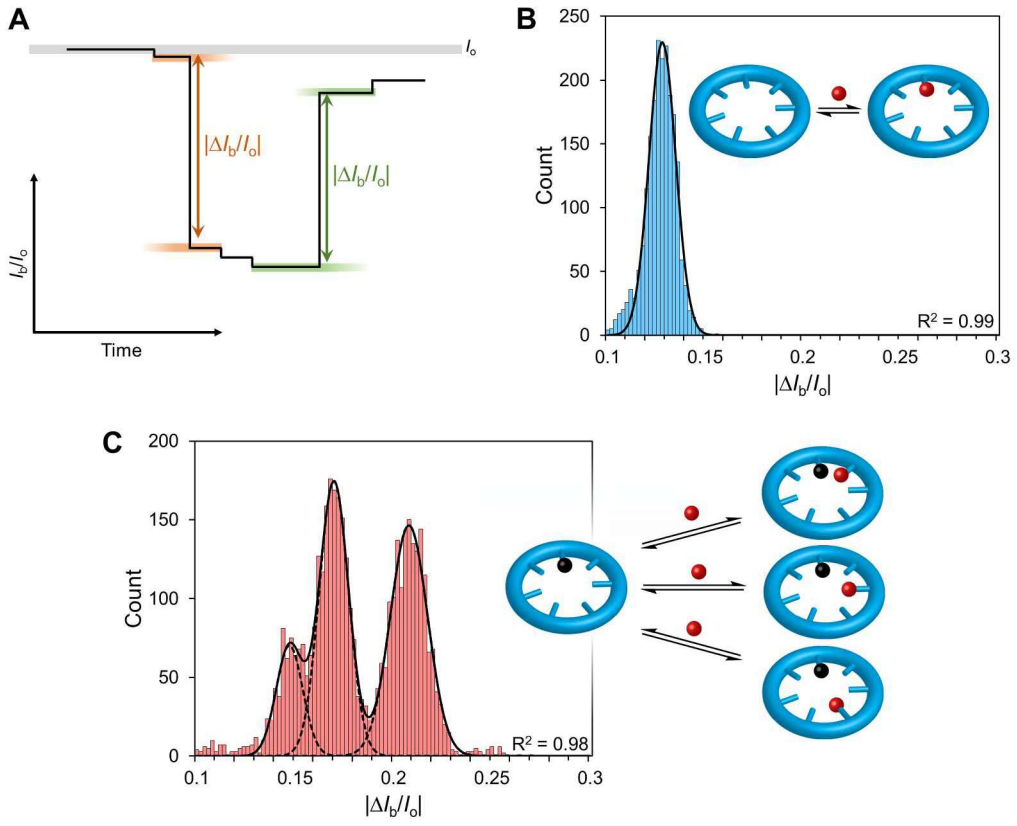


**Figure 6** **(A)** Illustrative ion current trace, indicating the major changes in residual ion current ($|\Delta I_b/I_o|$) arising from forward (orange) and reverse (green) reactions occurring specifically at constriction site-lysine residues. The experimentally observed $|\Delta I_b/I_o|$ values are plotted as frequency histograms for transitions between (**B**) 0 ⇌ 1 iminoboronate, and (**C**) 1 ⇌ 2 iminoboronate modifications at the constriction site-lysine residues. Gaussian curves were fitted iteratively. Cartoon insets illustrate the possible transitions corresponding to the observed histogram distributions.

A single distribution is seen in the major current changes ($|\Delta I_b/I_o|$) corresponding to $0 \rightleftharpoons 1$ iminoboronates at the constriction-site lysines, which is expected, since all seven lysine reactive sites are identical (Figure 6B). The formation of a second iminoboronate can occur in three positions relative to the first iminoboronate: adjacent, one lysine apart, or two lysine residues apart (Figure 6C inset), and pleasingly, three distributions emerge in the histogram data (Figure 6C). The unequal distribution of the transitions (in a 1 : 2.6 : 2.7 ratio) is not unexpected, since steric hindrance may lower the likelihood of adjacent iminoboronate formation.[56] Furthermore, the lower observed current change for the smaller peak is consistent with two closely packed modifications having a smaller cross-section compared to two well-separated iminoboronates. Performing a similar analysis for reactions involving $2 \rightleftharpoons 3$ iminoboronates is challenging as these events are both less frequent and involve 9 (likely overlapping) major current changes (Figure S43). Likewise, it should be noted that such analysis was not possible for the smaller blockages corresponding to iminoboronate formation at the *cis*-lysine ring, as the inherent noise variation in free pore current was much larger relative to such small current changes. Furthermore, the influence of *cis*-lysine iminoboronates on the current level (e.g. eclipsed or staggered displacement) cannot be accounted for (Figure S46). Nonetheless, the observed current changes reveal information about the symmetry of the nanopore, with the $1 \rightleftharpoons 2$ current transitions only being consistent with six- or seven-fold symmetry (Figure S42). The ubiquity of lysine residues means that reversible iminoboronate chemistry might be more widely exploited for probing the structures of other protein nanopores.

**Irreversible iminoboronate modification of an individual protein nanopore**

Following the successful characterization of the reactivity of the lysine residues within the channel of the nanopore using reversible covalent chemistry, we hoped that reductive amination might be employed to lock the lysine modifications in place. However, the reductive conditions required for such reactions were incompatible with the experimental set up; sodium borohydride led to disruption of the membrane (at 1 mM), whereas no reaction was observed with sodium triacetoxyborohydride or a range of organic reducing agents (pyridine borane, 2-methylpyridine borane and Hantzsch's ester), which also had very limited aqueous solubility. Therefore, an alternative approach was sought for the irreversible functionalization of amines. Amide formation between the lysine residues and an *N*-hydroxysuccinimide (NHS)-activated acid (3-sulfo-*N*-succinimidyl benzoate sodium salt, Figure 1C) was employed. Crucially, under the conditions employed, hydrolysis of the activated acid reagent was slower than the reaction with the lysine residues.

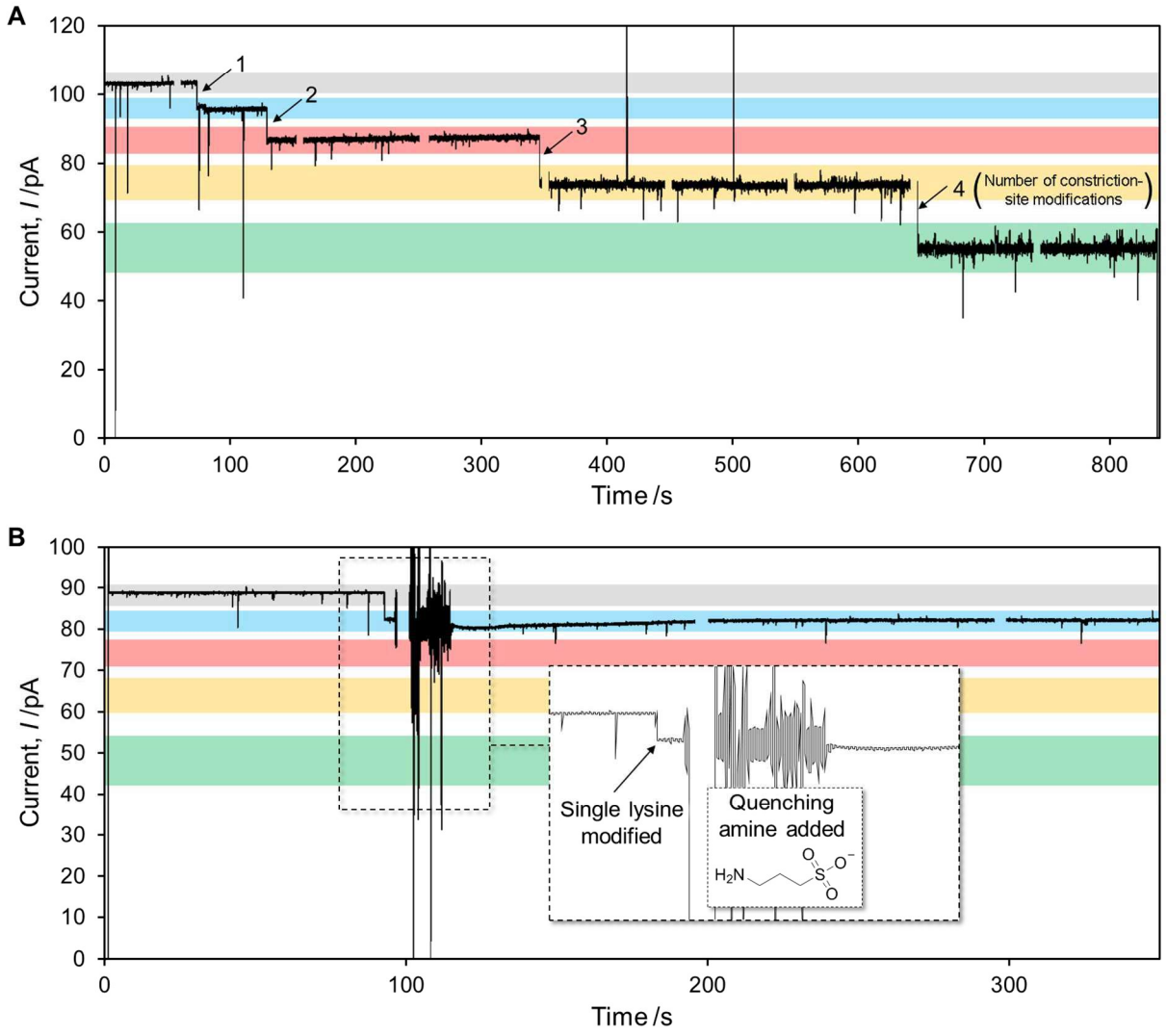


**Figure 7** Sample ion current traces (1 M KCl, 30 mM phosphate, pH 8.0, +100 mV, 298 K) generated on the addition of 3-sulfo-*N*-succinimidyl benzoate sodium salt to the *cis*-side of the bilayer. (**A**) Up to 4 large steps corresponding to successive constriction-site lysine modification are clearly visible. (**B**) Ion current trace in which the reagent was quenched following a single lysine modification.

Upon addition of a freshly made solution of 3-sulfo-*N*-succinimidyl benzoate sodium salt (final concentration ~3.2 μM) to the *cis*-side of the membrane under an applied potential of +100 mV, irreversible step-wise blockages of >8% in the ion current were observed (Figures 7A and S36). No pore modification was observed in control experiments with the unactivated acid and *N*-hydroxysuccinimide (Figure S39). Mirroring the findings of the reversible experiments (see sections above), repeat experiments found no more than four irreversible large current steps were observed, consistent with steric crowding of the reactive constriction-site lysine residues (Figures 7A, S36). It should be noted that the noise of the current increases with successive modifications, consistent with the increased number of conformational states facilitated by the flexible lysine side chains. Although four modifications increase the noise levels significantly, potentially limiting sensing applications of highly modified pores, a single modification results in only a small increase in noise.

The ability to observe pore modification in real time and to quench the reagent in response to the observed ion current changes meant that single lysine modifications within the channel of the pore could be attained. Accordingly, nanopores that were modified only once at the constriction-site (Figure S38) were reproducibly obtained by the addition of an excess of a water-soluble quenching amine (3-amino-1-propanesulfonic acid sodium salt) upon observation of a single (or other desired number) of modification(s) (Figures 7B, inset, S37). Thus, we have demonstrated that controlled functionalization of assignable lysine residues within the channel of the wild-type protein nanopore was indeed possible.

## Conclusions

We have demonstrated the feasibility of *in situ* synthetic modification of lysine residues within the channel of a membrane-bound wild-type α-HL nanopore. The approach provides a powerful and accessible alternative to genetic modification for introducing abiotic functionality. Initially, we utilized reversible iminoboronate reactions and the resulting changes in the ion current to probe the reactivity of the lysine residues within the channel of a single α-HL protein nanopore. Crucially, modifications to the exterior of the nanopore that could not be observed, were shown not to affect the integrity of the nanopore. In contrast, reversible reactions occurring at the rings of lysine residues at both the *cis*- and *trans*-openings, as well as the constriction site could be identified from the stepwise changes in the ion current flowing through the nanopore. Iminoboronate formation at the constriction-site lysine ring was observed regardless of which side of the pore reagents were added to. However, the *cis*- and *trans*- lysine rings were only modified when reagents were added to the respective side of the membrane. The reversible nature of the iminoboronate reaction enabled the rapid generation of a large amount of reactivity data. Statistical analysis of this data enabled the determination of the kinetics of iminoboronate formation at a single constriction-site lysine residue, as well as the identification of both the number and the relative positions of iminoboronate modifications at the constriction site. We subsequently utilized amide formation for the irreversible modification of lysine residues within the channel. Singly modified channels could be reproducibly obtained by using the real-time changes in the ion current accompanying lysine modification to inform the addition of a quenching agent to prevent further modification. Moreover, the statistical data from the initial investigation of reversible reactions enabled the positions of the irreversibly modified lysine residues to be assigned (*cis*-, *trans*- or constriction site). We anticipate that this approach will

provide a convenient and accessible route to the introduction of increasingly sophisticated functionalities for nanopore sensing applications, and possibly for the construction of transmembrane molecular machines.[57]

## Methods

### Single channel experiment set up

Single channel experiments were performed in a custom-built cell (Figure S1 and associated text). A hanging drop of hexadecane in *n*-pentane (5 μL, 10%, *v*/*v*) was touched on each side of the Teflon sheet containing an aperture and allowed to dry for 1 minute. KCl/potassium phosphate buffer (600 μL) was added to the well each side of the aperture. Lipid (1,2-diphytanoyl-*sn*-glycero-3-phosphocholine) (approx. 8 μL, 10 μg $\mu L^{-1}$) was added to each side of the well, and left for approx. 5 mins to allow the pentane to evaporate The cell was subsequently placed into a Faraday cage and Ag/AgCl electrodes (Warner), connected to a patch clamp amplifier (Axopatch 200B, Molecular Devices), were suspended either side of the Teflon sheet. The buffer solution on both sides of the Teflon sheet was aspirated and dispensed using a Hamilton syringe to 'paint' a phospholipid bilayer across the aperture. A ±1 mV pulse was applied at 1333 Hz to determine when a bilayer was obtained (capacitance of 40 to 70 pF). The membrane was characterised with successive 2 second sweeps under an applied potential ranging from +100 to −100 mM. The membrane was deemed acceptable if the range of current flow across the membrane measured <1 pA. A gel loading tip fitted to a 20 μL pipette was introduced into an aqueous solution of α-HL (approx. 250 μM (5 μL of the storage solution diluted with 45 μL of water)), without aspirating, such that a tiny amount (<1 μL) of the solution remained on the tip. The α-HL was then fired at the aperture. If after 10 minutes, no channel insertion was observed, then this process was repeated until a single-channel arose (Figure S2).

**Reversible pore modification**

The appropriate molecule (20 μL of a 0.1 mM solution) was added to either the *cis*- (under +100 mV applied potential) or *trans*- (under −100 mV applied potential) side of the membrane as appropriate. All data were collected using the patch clamp amplifier, and digitised (Axon Instruments Digidata 1332A) at a sample rate of 50 kHz. Single-channel ion current recordings were processed with Clampex 10.2 and Clampfit 10.2 software. All data was recorded at +/−100 mV in 100 second sweeps. At the start and end of each sweep the applied potential was reduced to 0 mV.

**Irreversible pore modification**

3-Sulfo-*N*-succinimidyl benzoate sodium salt (20 μL of a 0.1 M solution) was added to either the *cis*-side of the membrane under an applied +100 mV transmembrane potential. The contents of the well were mixed (5 × 50 μL). Single modifications could be visualised as ion current steps in real time. In order to achieve a single modification, after the first modification was observed, 3-amino-1-propanesulfonic acid sodium salt (20 μL of a 1 M solution) was added to the *cis*-side of the membrane and mixed (5 × 50 μL). All data were collected using the patch clamp amplifier, and digitised (Axon Instruments Digidata 1332A) at a sample rate of 50 kHz. Single-channel ion current recordings were processed with Clampex 10.2 and Clampfit 10.2 software. All data was recorded at +/−100 mV in 100 second sweeps. At the start and end of each sweep the applied potential was reduced to 0 mV.

**Data processing**

Single-channel ion current recordings were processed with Clampex 10.2 and Clampfit 10.2 software. Data was baseline corrected and filtered with a Lowpass Bessel (8-pole) filter with a 200 or 50 Hz cut-off for trace presentation and single-channel analysis respectively. The traces were then analysed with a single-channel search protocol, ignoring level changes of <1 ms. The results of the single-channel search were exported into Microsoft Excel 2013 for further processing, such as isolating step changes between certain levels. Gaussian curves and exponential decays were fitted iteratively using the solver package to minimize the residuals between fitted and experimental data.

## ASSOCIATED CONTENT

The following files are available free of charge.

Supporting Information contains experimental procedures, additional data, and modeled structures. (PDF)

## AUTHOR INFORMATION

**Corresponding Author**

*scott.cockroft@ed.ac.uk

**Author Contributions**

The manuscript was written through contributions of all authors. All authors have given approval to the final version of the manuscript.

**Funding Sources**

ERC Starting Grant 336935, “Transmembrane molecular machines”

ACKNOWLEDGMENT

We thank the Edinburgh Protein Purification Facility for equipment access and ERC Starting Grant 336935, “Transmembrane molecular machines” for funding.

REFERENCES

(1) Bayley, H.; Cremer, P. S., Stochastic Sensors Inspired by Biology. *Nature* **2001**, *413*, 226-230.
(2) Schmidt, J., Stochastic Sensors. *J. Mater. Chem.* **2005**, *15*, 831-840.
(3) Cooper, J. A.; Borsley, S.; Lusby, P. J.; Cockroft, S. L., Discrimination of Supramolecular Chirality Using a Protein Nanopore. *Chem. Sci.* **2017**, *8*, 5005-5009.
(4) Ying, Y.-L.; Zhang, J.; Meng, F.-N.; Cao, C.; Yao, X.; Willner, I.; Tian, H.; Long, Y.-T., A Stimuli-Responsive Nanopore Based on a Photoresponsive Host-Guest System. *Sci. Rep.* **2013**, *3*, 1662.
(5) Shin, S.-H.; Luchian, T.; Cheley, S.; Braha, O.; Bayley, H., Kinetics of a Reversible Covalent-Bond-Forming Reaction Observed at the Single-Molecule Level. *Angew. Chem. Int. Ed.* **2002**, *41*, 3707-3709.
(6) Wu, H.-C.; Bayley, H., Single-Molecule Detection of Nitrogen Mustards by Covalent Reaction within a Protein Nanopore. *J. Am. Chem. Soc.* **2008**, *130*, 6813-6819.
(7) Steffensen, M. B.; Rotem, D.; Bayley, H., Single-Molecule Analysis of Chirality in a Multicomponent Reaction Network. *Nat. Chem.* **2014**, *6*, 603-607.
(8) Lee, J.; Bayley, H., Semisynthetic Protein Nanoreactor for Single-Molecule Chemistry. *Proc. Natl. Acad. Sci. USA* **2015**, *112*, 13768-13773.
(9) Miles, B. N.; Ivanov, A. P.; Wilson, K. A.; Dogan, F.; Japrung, D.; Edel, J. B., Single Molecule Sensing with Solid-State Nanopores: Novel Materials, Methods, and Applications. *Chem. Soc. Rev.* **2013**, *42*, 15-28.
(10) Dekker, C., Solid-State Nanopores. *Nat. Nano.* **2007**, *2*, 209-215.
(11) C. Hulteen, J.; Martin, C. R., A General Template-Based Method for the Preparation of Nanomaterials. *J. Mater. Chem.* **1997**, *7*, 1075-1087.
(12) Spohr, R. In *Ion Tracks and Microtechnology: Principles and Applications*; Bethge, K., Ed.; Vieweg+Teubner Verlag: Wiesbaden, 1990, pp 183-210.
(13) Yameen, B.; Ali, M.; Neumann, R.; Ensinger, W.; Knoll, W.; Azzaroni, O., Synthetic Proton-Gated Ion Channels via Single Solid-State Nanochannels Modified with Responsive Polymer Brushes. *Nano Lett.* **2009**, *9*, 2788-2793.
(14) Yameen, B.; Ali, M.; Neumann, R.; Ensinger, W.; Knoll, W.; Azzaroni, O., Proton-Regulated Rectified Ionic Transport through Solid-State Conical Nanopores Modified with Phosphate-Bearing Polymer Brushes. *Chem. Commun.* **2010**, *46*, 1908-1910.
(15) Ali, M.; Ramirez, P.; Nguyen, H. Q.; Nasir, S.; Cervera, J.; Mafe, S.; Ensinger, W., Single Cigar-Shaped Nanopores Functionalized with Amphoteric Amino Acid Chains: Experimental and Theoretical Characterization. *ACS Nano* **2012**, *6*, 3631-3640.
(16) Storm, A. J.; Chen, J. H.; Ling, X. S.; Zandbergen, H. W.; Dekker, C., Fabrication of Solid-State Nanopores with Single-Nanometre Precision. *Nat. Mater.* **2003**, *2*, 537-540.

(17) Janssen, X. J. A.; Jonsson, M. P.; Plesa, C.; Soni, G. V.; Dekker, C.; Dekker, N. H., Rapid Manufacturing of Low-Noise Membranes for Nanopore Sensors by Trans-Chip Illumination Lithography. *Nanotechnology* **2012**, *23*, 475302.
(18) Li, J.; Stein, D.; McMullan, C.; Branton, D.; Aziz, M. J.; Golovchenko, J. A., Ion-Beam Sculpting at Nanometre Length Scales. *Nature* **2001**, *412*, 166-169.
(19) Zharov, I.; Khabibullin, A., Surface-Modified Silica Colloidal Crystals: Nanoporous Films and Membranes with Controlled Ionic and Molecular Transport. *Acc. Chem. Res.* **2014**, *47*, 440-449.
(20) Wan, Y.; Zhao, On the Controllable Soft-Templating Approach to Mesoporous Silicates. *Chem. Rev.* **2007**, *107*, 2821-2860.
(21) Soler-Illia, G. J. A. A.; Azzaroni, O., Multifunctional Hybrids by Combining Ordered Mesoporous Materials and Macromolecular Building Blocks. *Chem. Soc. Rev.* **2011**, *40*, 1107-1150.
(22) Soler-Illia, G. J. d. A. A.; Sanchez, C.; Lebeau, B.; Patarin, J., Chemical Strategies to Design Textured Materials: From Microporous and Mesoporous Oxides to Nanonetworks and Hierarchical Structures. *Chem. Rev.* **2002**, *102*, 4093-4138.
(23) Mehdi, A.; Reye, C.; Corriu, R., From Molecular Chemistry to Hybrid Nanomaterials. Design and Functionalization. *Chem. Soc. Rev.* **2011**, *40*, 563-574.
(24) Sanchez, C.; Boissière, C.; Grosso, D.; Laberty, C.; Nicole, L., Design, Synthesis, and Properties of Inorganic and Hybrid Thin Films Having Periodically Organized Nanoporosity. *Chem. Mat.* **2008**, *20*, 682-737.
(25) Anderson, B. N.; Muthukumar, M.; Meller, A., Ph Tuning of DNA Translocation Time through Organically Functionalized Nanopores. *ACS Nano* **2013**, *7*, 1408-1414.
(26) Wanunu, M.; Meller, A., Chemically Modified Solid-State Nanopores. *Nano Lett.* **2007**, *7*, 1580-1585.
(27) Tagliazucchi, M. In *Chemically Modified Nanopores and Nanochannels*; William Andrew Publishing: Boston, 2017, pp 1-25.
(28) Jovanovic-Talisman, T.; Tetenbaum-Novatt, J.; McKenney, A. S.; Zilman, A.; Peters, R.; Rout, M. P.; Chait, B. T., Artificial Nanopores That Mimic the Transport Selectivity of the Nuclear Pore Complex. *Nature* **2009**, *457*, 1023-1027.
(29) de Groot, G. W.; Santonicola, M. G.; Sugihara, K.; Zambelli, T.; Reimhult, E.; Vörös, J.; Vancso, G. J., Switching Transport through Nanopores with Ph-Responsive Polymer Brushes for Controlled Ion Permeability. *ACS Appl. Mater. Interfaces* **2013**, *5*, 1400-1407.
(30) Banghart, M.; Borges, K.; Isacoff, E.; Trauner, D.; Kramer, R. H., Light-Activated Ion Channels for Remote Control of Neuronal Firing. *Nat. Neurosci.* **2004**, *7*, 1381-1386.
(31) Mahendran, K. R.; Niitsu, A.; Kong, L.; Thomson, A. R.; Sessions, R. B.; Woolfson, D. N.; Bayley, H., A Monodisperse Transmembrane A-Helical Peptide Barrel. *Nat. Chem.* **2017**, *9*, 411-419.
(32) Hernandez-Ainsa, S.; Keyser, U. F., DNA Origami Nanopores: Developments, Challenges and Perspectives. *Nanoscale* **2014**, *6*, 14121-14132.
(33) Bell, N. A. W.; Engst, C. R.; Ablay, M.; Divitini, G.; Ducati, C.; Liedl, T.; Keyser, U. F., DNA Origami Nanopores. *Nano Lett.* **2012**, *12*, 512-517.
(34) Keyser, U. F., Enhancing Nanopore Sensing with DNA Nanotechnology. *Nat. Nano.* **2016**, *11*, 106-108.

(35) Song, L.; Hobaugh, M. R.; Shustak, C.; Cheley, S.; Bayley, H.; Gouaux, J. E., Structure of Staphylococcal α-Hemolysin, a Heptameric Transmembrane Pore. *Science* **1996**, *274*, 1859-1865.

(36) Gu, L.-Q.; Braha, O.; Conlan, S.; Cheley, S.; Bayley, H., Stochastic Sensing of Organic Analytes by a Pore-Forming Protein Containing a Molecular Adapter. *Nature* **1999**, *398*, 686-690.

(37) Wu, H.-C.; Astier, Y.; Maglia, G.; Mikhailova, E.; Bayley, H., Protein Nanopores with Covalently Attached Molecular Adapters. *J. Am. Chem. Soc.* **2007**, *129*, 16142-16148.

(38) Banerjee, A.; Mikhailova, E.; Cheley, S.; Gu, L.-Q.; Montoya, M.; Nagaoka, Y.; Gouaux, E.; Bayley, H., Molecular Bases of Cyclodextrin Adapter Interactions with Engineered Protein Nanopores. *Proc. Natl. Acad. Sci. USA* **2010**, *107*, 8165-8170.

(39) Li, W.-W.; Claridge, T. D. W.; Li, Q.; Wormald, M. R.; Davis, B. G.; Bayley, H., Tuning the Cavity of Cyclodextrins: Altered Sugar Adaptors in Protein Pores. *J. Am. Chem. Soc.* **2011**, *133*, 1987-2001.

(40) Howorka, S.; Bayley, H. In *In Vitro Mutagenesis Protocols*; Braman, J., Ed.; Humana Press: Totowa, NJ, 2002, pp 139-147.

(41) Spicer, C. D.; Davis, B. G., Selective Chemical Protein Modification. *Nat. Commun.* **2014**, *5*, 4740.

(42) Shin, S.-H.; Steffensen, M. B.; Claridge, T. D. W.; Bayley, H., Formation of a Chiral Center and Pyrimidal Inversion at the Single-Molecule Level. *Angew. Chem. Int. Ed.* **2007**, *46*, 7412-7416.

(43) Lee, J.; Boersma, A. J.; Boudreau, M. A.; Cheley, S.; Daltrop, O.; Li, J.; Tamagaki, H.; Bayley, H., Semisynthetic Nanoreactor for Reversible Single-Molecule Covalent Chemistry. *ACS Nano* **2016**, *10*, 8843-8850.

(44) Balabanova, L.; Golotin, V.; Podvolotskaya, A.; Rasskazov, V., Genetically Modified Proteins: Functional Improvement and Chimeragenesis. *Bioengineered* **2015**, *6*, 262-274.

(45) Blake, S.; Mayer, T.; Mayer, M.; Yang, J., Monitoring Chemical Reactions by Using Ion-Channel-Forming Peptides. *ChemBioChem* **2006**, *7*, 433-435.

(46) Boutureira, O.; Bernardes, G. J. L., Advances in Chemical Protein Modification. *Chem. Rev.* **2015**, *115*, 2174-2195.

(47) Baslé, E.; Joubert, N.; Pucheault, M., Protein Chemical Modification on Endogenous Amino Acids. *Chem. Biol.* **2010**, *17*, 213-227.

(48) Glebe, U.; Santos de Miranda, B.; van Rijn, P.; Boker, A. In *Bio-Synthetic Hybrid Materials and Bionanoparticles: A Biological Chemical Approach Towards Material Science*; The Royal Society of Chemistry: 2015, pp 1-29.

(49) Wloka, C.; Van Meervelt, V.; van Gelder, D.; Danda, N.; Jager, N.; Williams, C. P.; Maglia, G., Label-Free and Real-Time Detection of Protein Ubiquitination with a Biological Nanopore. *ACS Nano* **2017**, *11*, 4387-4394.

(50) Gouaux, J. E.; Braha, O.; Hobaugh, M. R.; Song, L.; Cheley, S.; Shustak, C.; Bayley, H., Subunit Stoichiometry of Staphylococcal α-Hemolysin in Crystals and on Membranes: A Heptameric Transmembrane Pore. *Proc. Natl. Acad. Sci. USA* **1994**, *91*, 12828-12831.

(51) Cal, P. M. S. D.; Vicente, J. B.; Pires, E.; Coelho, A. V.; Veiros, L. s. F.; Cordeiro, C.; Gois, P. M. P., Iminoboronates: A New Strategy for Reversible Protein Modification. *J. Am. Chem. Soc.* **2012**, *134*, 10299-10305.

(52) Bandyopadhyay, A.; Gao, J., Iminoboronate-Based Peptide Cyclization That Responds to Ph, Oxidation, and Small Molecule Modulators. *J. Am. Chem. Soc.* **2016**, *138*, 2098-2101.

(53) Bandyopadhyay, A.; McCarthy, K. A.; Kelly, M. A.; Gao, J., Targeting Bacteria Via Iminoboronate Chemistry of Amine-Presenting Lipids. *Nat. Commun.* **2015**, *6*, 6561.
(54) Cal, P. M. S. D.; Frade, R. F. M.; Chudasama, V.; Cordeiro, C.; Caddick, S.; Gois, P. M. P., Targeting Cancer Cells with Folic Acid-Iminoboronate Fluorescent Conjugates. *Chem. Commun.* **2014**, *50*, 5261-5263.
(55) Wanunu, M.; Sutin, J.; McNally, B.; Chow, A.; Meller, A., DNA Translocation Governed by Interactions with Solid-State Nanopores. *Biophys. J.* **2008**, *95*, 4716-4725.
(56) Plas, J.; Waghray, D.; Adisoejoso, J.; Ivasenko, O.; Dehaen, W.; de Feyter, S., Insights into Dynamic Covalent Chemistry at Surfaces. *Chem. Commun.* **2015**, *51*, 16338-16341.
(57) Watson, M. A.; Cockroft, S. L., Man-Made Molecular Machines: Membrane Bound. *Chem. Soc. Rev.* **2016**, *45*, 6118-6129.

GRAPHICAL TOC ENTRY: